BULLETIN OF THE POLISH ACADEMY OF SCIENCES
TECHNICAL SCIENCES, Vol. 63, No. 2, 2015
DOI: 10.1515/bpasts-2015-0053

Influence of convective heat and mass conditions in MHD flow of nanofluid

S.A. SHEHZAD[1]*, T. HAYAT[2,3], and A. ALSAEDI[3]

[1] Department of Mathematics, Comsats Institute of Information Technology, Sahiwal 57000, Pakistan
[2] Department of Mathematics, Quaid-i-Azam University 45320, Islamabad 44000, Pakistan
[3] Nonlinear Analysis and Applied Mathematics (NAAM) Research Group, Faculty of Science, King Abdulaziz University, Jeddah, Saudi Arabia

Abstract. This article aims to investigate the two-dimensional magnetohydrodynamic (MHD) boundary layer flow of nanofluid. Convective mass condition is introduced. Analysis has been discussed in the presence of an applied magnetic field. The Brownian motion and thermophoresis effects are incorporated. The arising nonlinear problems are first converted to ordinary differential equations and then series solutions are constructed. Convergence of series solutions is examined through plots and numerical values. Results are plotted and discussed for the temperature and concentration. Numerical computations for skin-friction coefficient, local Nusselt and Sherwood numbers are performed and analyzed. Comparison with the previous limiting case is noted in an excellent agreement.

Key words: nanofluid, MHD flow; convective mass condition, nonlinear analysis, HAM.

1. Introduction

In recent times, the sustainable energy generation has been a very serious issue across the globe. Solar energy perhaps has a reasonable solution with the hourly solar flux incident on the earth's surface being greater than all the consumption of energy in a year. Solar energy is also known as a best source of renewable energy with the minimal environmental impact [1]. Power tower solar collectors are more effective through the use of nanofluid as a working fluid. On the other hand, the magnetohydrodynamic (MHD) nanofluid has key importance in engineering, physics and chemistry. Specifically such fluids have wide coverage in the optical modulators, tunable optical fiber filters, optical grating, optical switches, polymer industry, stretching of plastic sheets and metallurgy. Several metallurgical processes involve the cooling of continuous strips or filaments by drawing them through a nanofluid. Such strips in processes of drawing, thinning of copper wires and annealing are sometimes stretched. The quality and desired characteristics of a final product in such cases strongly depend upon the cooling rate by drawing such strips in an electrically conducting fluid. The magnetic nanoparticles are also useful in the construction of loudspeakers, magnetic cell separation, hyperthermia, drug delivery etc. Recently, the nanofluids in view of their enhanced thermal characteristics have been attracted by the scientists and engineers. It is known well established fact that the nanofluids improve the heat transfer performance of many engineering applications. In fact the traditional fluids like oil, water and ethylene glycol mixture are poor heat transfer liquids. The thermal conductivity of such traditional liquids affects the heat transfer coefficient between the heat transfer medium and heat transfer surface. Various techniques have been utilized to enhance the thermal conductivity of traditional fluids by suspending nano/micro or large-sized particles in the liquid [2]. The addition of nanoparticles in the traditional liquid is very popular amongst such techniques [3]. As pointed out by Choi et al. [4], the thermal conductivity of the fluid through such technique has been improved approximately two times. After such pioneering research, numerous theoretical and experimental attempts have been made on this topic. For example, Makinde and Aziz [5] investigated the boundary layer flow of nanofluid with the convective type temperature condition. The analysis of Makinde et al. [5] was extended by Alsaedi et al. [6] by considering the stagnation point flow and heat source/sink effects. Entropy generation analysis in the steady flow of nanofluid with a magnetic field was presented by Rashidi et al. [7]. Turkyilmazoglu [8] provided an exact solution to MHD flow of nanofluid with a slip condition. Series solutions for the boundary layer flow of nanofluid over an exponentially stretching surface were given by Nadeem and Lee [9]. Mixed convection stagnation point flow of nanofluid over a stretching/shrinking sheet was numerically examined by Makinde et al. [10]. Stagnation point flow of nanofluid over an exponentially stretching sheet was studied by Mustafa et al. [11]. The authors have developed both numerical and series solutions. Mutuku-Njane and Makinde [12] addressed the simultaneous effects of buoyancy force and Navier slip in magnetohydrodynamic flow of nanofluid over a convectively heated plate. Newtonian heating and viscous dissipation effects in boundary layer flow of viscous nanofluid were explored by Makinde [13]. Makinde [14] also discussed the unsteady flow of viscous nanofluid over a surface with convective boundary condition. Kuznetson and Nield [15] provided

---

*e-mail: ali_qau70@yahoo.com

a revised model of Cheng-Minkowycz problem for natural convection boundary layer flow of nanofluid. Very recently, Mutuku-Njane and Makinde [16] studied the MHD flow of nanofluid with convective thermal condition.

Boundary layer flow with heat and mass transfer is an important area of research in fluid dynamics because it occurs in many chemical and engineering processes like glass-fiber and paper production, manufacturing of materials by extrusion, hot rolling, polymer sheets and filaments, annealing and thinning of copper wires, cooling of large metallic plate in a bath etc. In view of all these technological and engineering applications, there exist ample attempts, for example see [17–23]. In continuation, Turkyilmazoglu and Pop [24] analyzed the Soret and heat generation effects on MHD free-convection flow over an impulsively infinite vertical plate. They also examined the radiation effects for two different types of thermal boundary conditions in this study. Entropy generation analysis in an unsteady MHD flow over a stretched rotating disk was studied by Rashidi et al. [25]. Rundora and Makinde [26] numerically analyzed the influence of suction/injection on the variable viscosity non-Newtonian fluid in a channel with convective type heat condition. Recently, Shehzad et al. [27] analytically studied the hydromagnetic three-dimensional flow of Maxwell fluid with heat generation/absorption. They discussed the flow situation through prescribed surface temperature and prescribed surface heat flux.

It has been noticed that the heat transfer analysis in the past has been mostly dealt with the boundary condition either through prescribed temperature or heat flux at the surface. Few studies in this direction are made using temperature convective condition at the surface instead of prescribed surface temperature or heat flux. However, no attempt is yet presented for the convective mass condition at the surface. This study introduces such a condition in the literature. Even such a condition has not been utilized yet in flow analysis without nanoparticles. Thus, the present discusses the flow of nanofluid over a stretching surface. The convective conditions through temperature and concentration are imposed on the surface. The governing dimensionless nonlinear ordinary differential equations are solved analytically by employing the homotopy analysis method (HAM) [28–38] and results are presented in the forms of series. Graphs of various interesting physical parameters are plotted for the temperature and concentration fields. The physical quantities of interest namely the local skin-friction coefficient and local Nusselt and Sherwood numbers are computed numerically.

2. Problems development

We consider the two-dimensional $(x,\, y)$ steady MHD flow of nanofluid over a stretching surface. Convective heat and mass conditions are taken into account. It is further assumed that the surface of sheet is heated by a hot fluid has temperature T_f and concentration C_f that give heat and mass transfer coefficients h_1 and h_2. The magnetic field of strength B_0 is applied normal to the flow field (see Fig. 1). The magnetic Reynolds number is chosen small. As a consequence the induced magnetic field is smaller in comparison to the applied magnetic field. Thus, the induced magnetic field is not considered. Effects of viscous dissipation and Joule heating are further considered. The two-dimensional MHD equations for viscous nanofluid are given by

$$\frac{\partial u}{\partial x}+\frac{\partial v}{\partial y}=0, \tag{1}$$

$$\begin{aligned} u\frac{\partial u}{\partial x}+v\frac{\partial u}{\partial y}&=-\frac{1}{\rho_f}\frac{\partial p}{\partial x}\\ &+\nu\left(\frac{\partial^2 u}{\partial x^2}+\frac{\partial^2 u}{\partial y^2}\right)-\frac{\sigma B_0^2}{\rho_f}u, \end{aligned} \tag{2}$$

$$u\frac{\partial v}{\partial x}+v\frac{\partial v}{\partial y}=-\frac{1}{\rho_f}\frac{\partial p}{\partial y}+\nu\left(\frac{\partial^2 v}{\partial x^2}+\frac{\partial^2 v}{\partial y^2}\right), \tag{3}$$

$$\begin{aligned} u\frac{\partial T}{\partial x}+v\frac{\partial T}{\partial y}&=\alpha\left(\frac{\partial^2 T}{\partial x^2}+\frac{\partial^2 T}{\partial y^2}\right)\\ &+\tau\left(\begin{array}{c} D_B\left(\frac{\partial C}{\partial x}\frac{\partial T}{\partial x}+\frac{\partial C}{\partial y}\frac{\partial T}{\partial y}\right)\\ +\frac{D_T}{T_\infty}\left(\left(\frac{\partial T}{\partial x}\right)^2+\left(\frac{\partial T}{\partial y}\right)^2\right)\end{array}\right)\\ +\frac{\nu}{c_f}&\left(2\left(\frac{\partial u}{\partial x}\right)^2+2\left(\frac{\partial v}{\partial y}\right)^2+\left(\frac{\partial u}{\partial y}+\frac{\partial v}{\partial x}\right)^2\right)+\frac{\sigma B_0^2}{(\rho c)_f}u^2, \end{aligned} \tag{4}$$

$$\begin{aligned} u\frac{\partial C}{\partial x}+v\frac{\partial C}{\partial y}&=D_B\left(\frac{\partial^2 C}{\partial x^2}+\frac{\partial^2 C}{\partial y^2}\right)\\ &+\frac{D_T}{T_\infty}\left(\frac{\partial^2 T}{\partial x^2}+\frac{\partial^2 T}{\partial y^2}\right). \end{aligned} \tag{5}$$

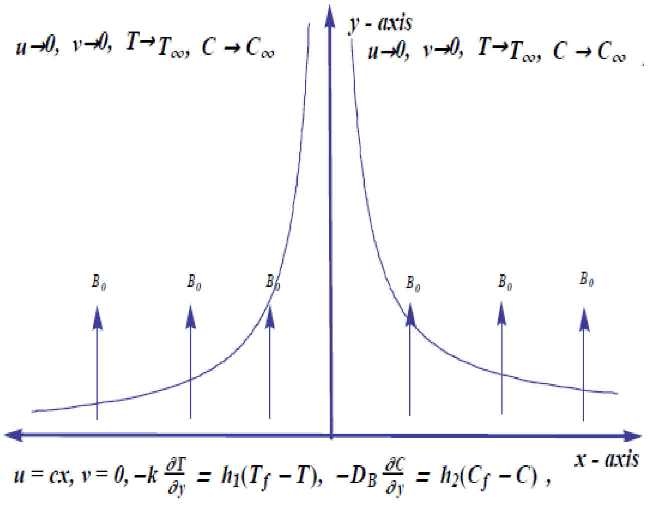

Fig. 1. Physical model

The boundary conditions for the considered flow analysis are

$$\begin{aligned} u=u_w(x)=cx,\quad v=0,\quad -k\frac{\partial T}{\partial y}=h_1(T_f-T),\\ -D_B\frac{\partial C}{\partial y}=h_2(C_f-C),\quad \text{at}\quad y=0, \end{aligned} \tag{6}$$

$$u\to 0,\quad T\to T_\infty,\quad C\to C_\infty,\quad \text{when}\quad y\to\infty, \tag{7}$$

where u and v are the velocity components in the $x-$ and $y-$directions, p the fluid pressure, ρ_f the density of fluid,

ν the kinematic viscosity, σ the Steffan-Boltzman constant, α the thermal diffusivity, $\tau = \dfrac{(\rho c)_p}{(\rho c)_f}$ the ratio of nanoparticle heat capacity and the base fluid heat capacity, D_B the Brownian diffusion coefficient, D_T the thermophoretic diffusion coefficient, k the thermal conductivity, h_1 and h_2 the heat and mass transfer coefficients, T_f and C_f the temperature and concentration of fluid and T_∞ and C_∞ are the ambient fluid temperature and concentration.

Equations (2)–(7) can be reduced into the dimensionless form by introducing the following new variables:

$$\begin{gathered} u = cxf'(\eta), \quad v = -\sqrt{c\nu}f(\eta), \quad \eta = y\sqrt{\frac{c}{\nu}}, \\ \theta(\eta) = \frac{T - T_\infty}{T_f - T_\infty}, \quad \phi(\eta) = \frac{C - C_\infty}{C_f - C_\infty}. \end{gathered} \tag{8}$$

By employing the boundary layer assumptions [39], we have $\frac{\partial p}{\partial y} = 0$. In above expression, η the dimensionless variable and f, θ and ϕ are the dimensionless velocity, temperature and concentration, respectively. Thus by neglecting pressure gradient in the y-direction, the equation of linear momentum, energy and concentration in dimensionless form become

$$f''' + ff'' - f'^2 - M^2 f' = 0, \tag{9}$$

$$\begin{gathered} \theta'' + \Pr f\theta' + \Pr Nb\theta'\phi' + \Pr Nt\theta'^2 \\ + \Pr Ecf''^2 + \Pr EcM^2 f'^2 = 0, \end{gathered} \tag{10}$$

$$\phi'' + Lef\phi' + (Nt/Nb)\,\theta'' = 0, \tag{11}$$

$$\begin{gathered} f = 0, \quad f' = 1, \quad \theta' = -\gamma_1(1 - \theta(0)), \\ \phi' = -\gamma_2(1 - \phi(0)) \quad \text{at} \quad \eta = 0, \end{gathered} \tag{12}$$

$$f' \to 0, \quad \theta \to 0, \quad \phi \to 0 \quad \text{as} \quad \eta \to \infty, \tag{13}$$

where $M^2 = \sigma B_0^2/\rho_f c$ is the magnetic parameter, $\Pr = \nu/\alpha$ is the Prandtl number, $Le = \nu/D_B$ is the Lewis number, $Nb = (\rho c)_p D_B (C_f - C_\infty)/(\rho c)_f \nu$ is the Brownian motion parameter, $Nt = (\rho c)_p D_T (T_f - T_\infty)/(\rho c)_f \nu T_\infty$ is the thermophoresis parameter, $Ec = u_w^2/c_p(T_f - T_\infty)$ and $\gamma_1 = (h_1/k)\sqrt{\nu/a}$, $\gamma_2 = (h_2/D_B)\sqrt{\nu/a}$ are the Biot numbers. It is worth mentioning here that γ_1 and γ_2 are the heat transfer and mass transfer Biot numbers, respectively.

The skin friction coefficient, the local Nusselt number and the local Sherwood number are

$$\begin{gathered} C_f = \frac{\tau_w}{\rho_f u_w^2(x)}, \qquad Nu_x = \frac{xq_w}{k(T_f - T_\infty)}, \\ Sh_x = \frac{xq_m}{D_B(C_f - C_\infty)}, \end{gathered} \tag{14}$$

where τ_w is the shear stress along the stretching surface, q_w is the surface heat flux and q_m is the surface mass flux. The local skin-friction coefficient, local Nusselt and local Sherwood numbers in dimensionless forms are given below:

$$\begin{gathered} Re_x^{1/2} C_{fx} = f''(0), \quad Nu_x/Re_x^{1/2} = -\theta'(0), \\ Sh_x/Re_x^{1/2} = -\phi'(0), \end{gathered} \tag{15}$$

where $Re_x = u_w(x)x/\nu$ is the local Reynolds number.

3. Homotopy analysis solutions

Considering a set of base functions

$$\{\eta^k \exp(-n\eta), \qquad k \geq 0,\, n \geq 0\}$$

one can express f and θ as follows

$$f_m(\eta) = \sum_{n=0}^{\infty}\sum_{k=0}^{\infty} a_{m,\,n}^k \eta^k \exp(-n\eta), \tag{16}$$

$$\theta_m(\eta) = \sum_{n=0}^{\infty}\sum_{k=0}^{\infty} b_{m,\,n}^k \eta^k \exp(-n\eta), \tag{17}$$

$$\phi_m(\eta) = \sum_{n=0}^{\infty}\sum_{k=0}^{\infty} c_{m,\,n}^k \eta^k \exp(-n\eta), \tag{18}$$

in which $a_{m,\,n}^k$, $b_{m,\,n}^k$ and $c_{m,\,n}^k$ are the coefficients. The initial approximations and auxiliary linear operators are assumed in the forms:

$$\begin{gathered} f_0(\eta) = 1 - \exp(-\eta), \quad \theta_0(\eta) = \frac{\gamma_1 \exp(-\eta)}{1 + \gamma_1}, \\ \phi_0(\eta) = \frac{\gamma_2 \exp(-\eta)}{1 + \gamma_2}, \end{gathered} \tag{19}$$

$$L(f) = f''' - f', \quad L(\theta) = \theta'' - \theta, \quad L(\phi) = \phi'' - \phi, \tag{20}$$

with

$$\begin{gathered} L(f)(C_1 + C_2 e^\eta + C_3 e^{-\eta}) = 0, \\ L(\theta)(C_4 e^\eta + C_5 e^{-\eta}) = 0, \quad L(\phi)(C_6 e^\eta + C_7 e^{-\eta}) = 0, \end{gathered} \tag{21}$$

where C_i $(i = 1 - 7)$ are the arbitrary constants.

The problems at zeroth order deformation are

$$\begin{gathered} (1 - p)L(f)\left[\overline{f}(\eta;\, p) - f_0(\eta)\right] \\ = p\hbar_f \mathbf{N}_f\left[\overline{f}(\eta;\, p)\right], \end{gathered} \tag{22}$$

$$\begin{gathered} (1 - p)L(\theta)\left[\overline{\theta}(\eta;\, p) - \theta_0(\eta)\right] \\ = p\hbar_\theta \mathbf{N}_\theta\left[\overline{f}(\eta;\, p),\, \overline{\theta}(\eta,\, p),\, \bar{\phi}(\eta,\, p)\right], \end{gathered} \tag{23}$$

$$\begin{gathered} (1 - p)L(\phi)\left[\overline{\phi}(\eta;\, p) - \theta_0(\eta)\right] \\ = p\hbar_\theta \mathbf{N}_\theta\left[\overline{f}(\eta;\, p),\, \overline{\theta}(\eta,\, p),\, \overline{\phi}(\eta,\, p)\right], \end{gathered} \tag{24}$$

$$\begin{gathered} \overline{f}(0;\, p) = 0, \quad \overline{f}'(0;\, p) = 1, \\ \overline{\theta}'(0,\, p) = -\gamma_1(1 - \overline{\theta}(0,\, p)), \\ \overline{\phi}'(0,\, p) = -\gamma_2(1 - \overline{\phi}(0,\, p)), \end{gathered} \tag{25}$$

$$\overline{f}'(\infty;\, p) = 0, \quad \overline{\theta}(\infty,\, p) = 0, \quad \overline{\phi}(\infty,\, p) = 0, \tag{26}$$

$$\begin{gathered} \mathbf{N}_f[\overline{f}(\eta,\, p)] = \frac{\partial^3 \overline{f}(\eta,\, p)}{\partial \eta^3} + \overline{f}(\eta,\, p)\frac{\partial^2 \overline{f}(\eta,\, p)}{\partial \eta^2} \\ - \left(\frac{\partial \overline{f}(\eta,\, p)}{\partial \eta}\right)^2 - M^2 \frac{\partial \overline{f}(\eta,\, p)}{\partial \eta}, \end{gathered} \tag{27}$$

$$\begin{gathered} \mathbf{N}_\theta[\overline{\theta}(\eta,\, p),\, \overline{f}(\eta,\, p),\, \overline{\phi}(\eta,\, p)] = \frac{\partial^2 \overline{\theta}(\eta,\, p)}{\partial \eta^2} \\ + \Pr Nb \frac{\partial \overline{\theta}(\eta,\, p)}{\partial \eta}\frac{\partial \overline{\phi}(\eta,\, p)}{\partial \eta} + \Pr Nt\left(\frac{\partial \overline{\theta}(\eta,\, p)}{\partial \eta}\right)^2 \\ + \Pr Ec\left(\frac{\partial^2 \overline{f}(\eta,\, p)}{\partial \eta^2}\right)^2 + \Pr EcM^2\left(\frac{\partial \overline{f}(\eta,\, p)}{\partial \eta}\right)^2, \end{gathered} \tag{28}$$

$$\mathbf{N}_\theta[\overline{\phi}(\eta,\,p),\,\overline{f}(\eta,\,p),\,\overline{\theta}(\eta,\,p)] = \frac{\partial^2\overline{\phi}(\eta,\,p)}{\partial\eta^2} + Le\overline{f}(\eta,\,p)\frac{\partial\overline{\phi}(\eta,\,p)}{\partial\eta} + (Nt/Nb)\,\frac{\partial^2\overline{\theta}(\eta,\,p)}{\partial\eta^2}, \tag{29}$$

where $p \in [0,\,1]$ is an embedding parameter, $\hbar_f$, $\hbar_\theta$ and $\hbar_\phi$ are the non-zero auxiliary parameters and $\mathbf{N}_f$, $\mathbf{N}_\theta$ and $\mathbf{N}_\phi$ are the nonlinear operators. When $p = 0$ and $p = 1$ then we have

$$\begin{gathered}\overline{f}(\eta;\,0) = f_0(\eta), \quad \overline{\theta}(\eta,\,0) = \theta_0(\eta), \\ \overline{\phi}(\eta,\,0) = \phi_0(\eta) \quad \text{and} \quad \overline{f}(\eta;\,1) = f(\eta), \\ \overline{\theta}(\eta,\,1) = \theta(\eta), \quad \overline{\phi}(\eta,\,1) = \phi(\eta),\end{gathered} \tag{30}$$

and when p increases from 0 to 1 then $f(\eta,\,p)$, $\theta(\eta,\,p)$ and $\phi(\eta,\,p)$ vary from $f_0(\eta)$, $\theta_0(\eta)$, $\phi_0(\eta)$ to $f(\eta)$, $\theta(\eta)$ and $\phi(\eta)$. By Taylor series expansion one obtains

$$f(\eta,\,p) = f_0(\eta) + \sum_{m=1}^{\infty} f_m(\eta)p^m, \tag{31}$$

$$\theta(\eta,\,p) = \theta_0(\eta) + \sum_{m=1}^{\infty} \theta_m(\eta)p^m, \tag{32}$$

$$\phi(\eta,\,p) = \phi_0(\eta) + \sum_{m=1}^{\infty} \phi_m(\eta)p^m, \tag{33}$$

$$\begin{gathered}f_m(\eta) = \frac{1}{m!}\left.\frac{\partial^m f(\eta;\,p)}{\partial\eta^m}\right|_{p=0}, \\ \theta_m(\eta) = \frac{1}{m!}\left.\frac{\partial^m \theta(\eta;\,p)}{\partial\eta^m}\right|_{p=0}, \\ \phi_m(\eta) = \frac{1}{m!}\left.\frac{\partial^m \phi(\eta;\,p)}{\partial\eta^m}\right|_{p=0},\end{gathered} \tag{34}$$

where the convergence of above series strongly depends upon $\hbar_f$, $\hbar_\theta$ and $\hbar_\phi$. Considering that $\hbar_f$, $\hbar_\theta$ and $\hbar_\phi$ are selected properly such that (31)–(33) converge at $p = 1$ and then we have

$$f(\eta) = f_0(\eta) + \sum_{m=1}^{\infty} f_m(\eta), \tag{35}$$

$$\theta(\eta) = \theta_0(\eta) + \sum_{m=1}^{\infty} \theta_m(\eta), \tag{36}$$

$$\phi(\eta) = \phi_0(\eta) + \sum_{m=1}^{\infty} \phi_m(\eta). \tag{37}$$

The general solutions can be written as

$$f_m(\eta) = f_m^*(\eta) + C_1 + C_2e^{\eta} + C_3e^{-\eta}, \tag{38}$$

$$\theta_m(\eta) = \theta_m^*(\eta) + C_4e^{\eta} + C_5e^{-\eta}, \tag{39}$$

$$\phi_m(\eta) = \phi_m^*(\eta) + C_6e^{\eta} + C_7e^{-\eta}, \tag{40}$$

where f_m^*, θ_m^* and $\phi_m^*(\eta)$ are the special solutions.

4. Convergence of homtopy solutions and discussion

Obviously the auxiliary parameters $\hbar_f$, $\hbar_\theta$ and $\hbar_\phi$ appearing in the derived series solutions can adjust and control the convergence of the homotopy solutions. Hence, the $\hbar$-curves are plotted for 22^{nd}-order of approximations in order to determine the range of admissible values of $\hbar_f$, $\hbar_\theta$ and $\hbar_\phi$. Figure 2 confirms that the admissible values of $\hbar_f$, $\hbar_\theta$ and $\hbar_\phi$ are $-1.6 \le \hbar_f \le -0.08$, $-1.6 \le \hbar_\theta \le -0.5$, $-1.5 \le \hbar_\phi \le -0.4$. The series converges in the whole region of η when $\hbar_f = \hbar_\theta = \hbar_\phi = -1.0$ (see Table 1).

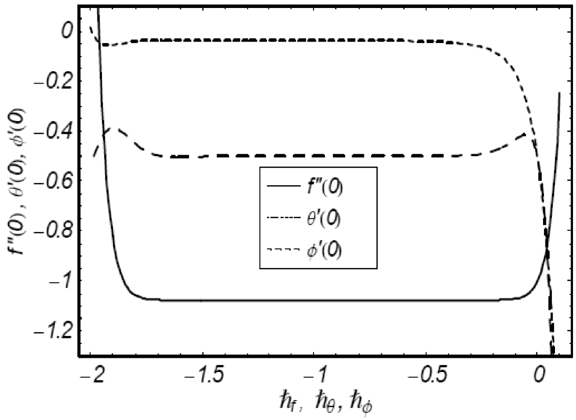

Fig. 2. $\hbar-$curves for functions $f(\eta)$, $\theta(\eta)$ and $\phi(\eta)$ at 22th order of approximations when $M = 0.4$, $\Pr = 0.9$, $Le = 2.0$, $Nt = Nb = 0.4$, $\gamma_1 = \gamma_2 = 1.0$ and $Ec = 0.8$

Table 1
Convergence of homotopy solution for different order of approximations when $M = 0.4$, $\Pr = 0.9$, $Le = 2.0$, $Nt = Nb = 0.4$, $\gamma_1 = \gamma_2 = 1.0$, $Ec = 0.8$ and $\hbar_f = \hbar_\theta = \hbar_\phi = -1.0$

Order of approximation	$-f''(0)$	$-\theta'(0)$	$-\phi'(0)$
1	1.08000	0.24330	0.32500
10	1.07703	0.04263	0.50080
20	1.07703	0.03833	0.50215
25	1.07703	0.03813	0.50223
31	1.07703	0.03807	0.50225
35	1.07703	0.03807	0.50225
40	1.07703	0.03807	0.50225
50	1.07703	0.03807	0.50225

Figure 3 is plotted to see the change in the velocity $f'(\eta)$ corresponding to different values of M. We have seen that the velocity and momentum boundary layer thickness are decreased. Lorentz force resists in fluid flow that leads to a reduction in the velocity. To analyze the variations of magnetic parameter M, Prandtl number $\Pr$, Biot numbers γ_1 and γ_2, thermophoresis parameter Nt, Brownian motion parameter Nb and Eckert number Ec on the dimensionless temperature $\theta(\eta)$, Figs. 4–10 are sketched. Figure 4 indicates that higher values of magnetic parameter increase the temperature. A magnetic parameter strongly depends upon the Lorentz force. The higher magnetic parameter has the stronger Lorentz force and the lower magnetic parameter corresponds to the weaker Lorentz force. The stronger Lorentz force creates more heat in the fluid that shows an increase in the temperature and thermal boundary layer thickness. Figure 5 shows that the temperature and thermal boundary layer thickness are reduced for smaller values of the Prandtl number. The Prandtl number is the ratio of momentum to thermal diffusivity. For the larger Prandtl number, the momentum diffusivity increases whereas the thermal diffusivity is decreased and for lower Prandtl fluids, momentum diffusivity is smaller in comparison to the thermal diffusivity. This stronger thermal diffusivity leads to a thicker thermal boundary layer thickness. An increase in the Biot number γ_1 corresponds to a higher temperature. From Fig. 6, we analyzed that the temperature is increasing rapidly for $\gamma_1 = 0.1$ to $\gamma_1 = 0.6, 1.2$ but for the values greater than 1.2, it increases slowly. From the definition of the Biot number γ_1, it is clear that the Biot number γ_1 involves the heat transfer coefficient h_1. For increasing values of the Biot number γ_1, the heat transfer coefficient increases which yields heat which leads to increase of temperature. The influence of Biot number γ_2 is examined in Fig. 7. Here one can see that both temperature and associated layer thickness increase by increasing Biot number γ_2. Biot number γ_2 has a great dependence on concentration transfer coefficient h_2. The concentration transfer coefficient h_2 is increased when we increase the values of Biot number γ_2 due to which the temperature and thermal boundary layer thickness are enhanced. Figures 8 and 9 illustrate the variations of thermophoresis and Brownian motion parameters on the dimensionless temperature. Temperature and thermal boundary layer thickness are enhanced with the increasing values of thermophoresis and Brownian motion parameters. An enhancement in the temperature due to Brownian motion parameter is more pronounced in comparison to the thermophoresis parameter. Figure 10 illustrates that the temperature and thermal boundary layer thickness are enhanced with an increase in the values of Eckert number.

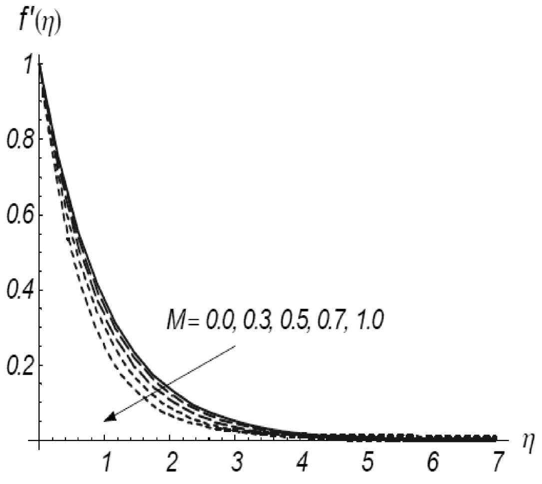

Fig. 3. Variation in velocity $f'(\eta)$ vs η for different values of M

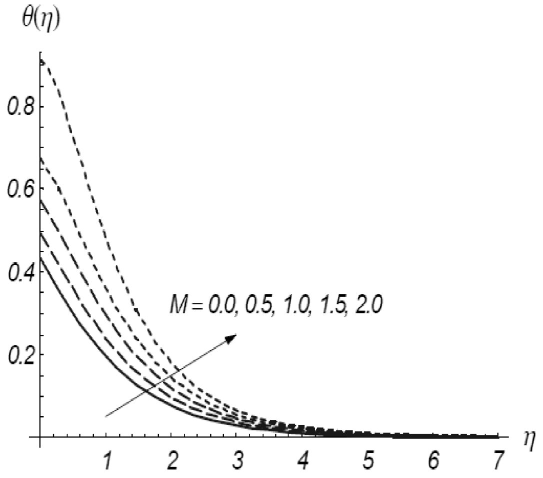

Fig. 4. Variation in temperature $\theta(\eta)$ vs η for different values of M when $\Pr = 0.9$, $Le = 3.0$, $\gamma_1 = \gamma_2 = 0.5$, $Nt = Nb = 0.5$ and $Ec = 0.8$

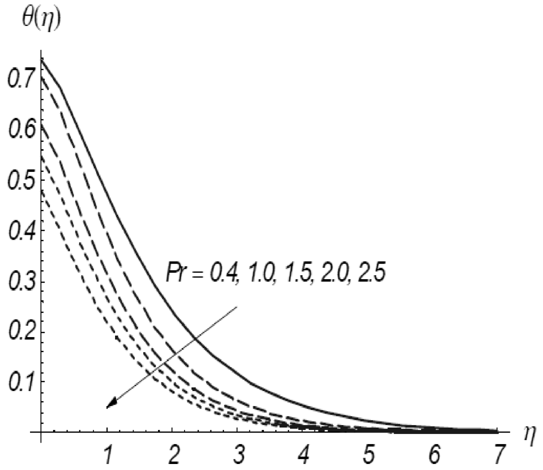

Fig. 5. Variation in temperature $\theta(\eta)$ vs η for different values of Pr when $M = 0.7$, $Le = 3.0$, $\gamma_1 = \gamma_2 = 0.5$, $Nt = Nb = 0.5$ and $Ec = 0.8$

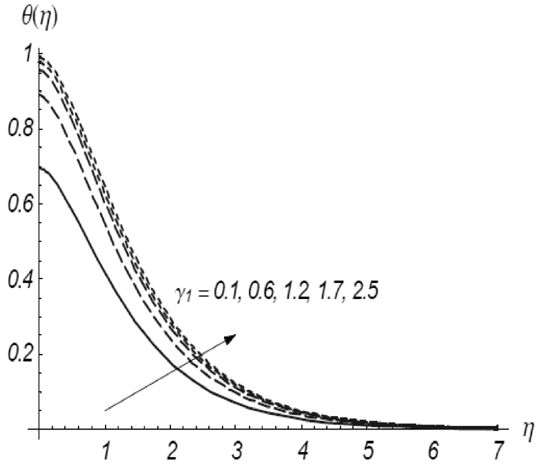

Fig. 6. Variation in temperature $\theta(\eta)$ vs η for different values of γ_1 when $M = 0.7$, $\Pr = 0.9$, $Le = 3.0$, $\gamma_2 = 0.5$, $Nt = Nb = 0.5$ and $Ec = 0.8$

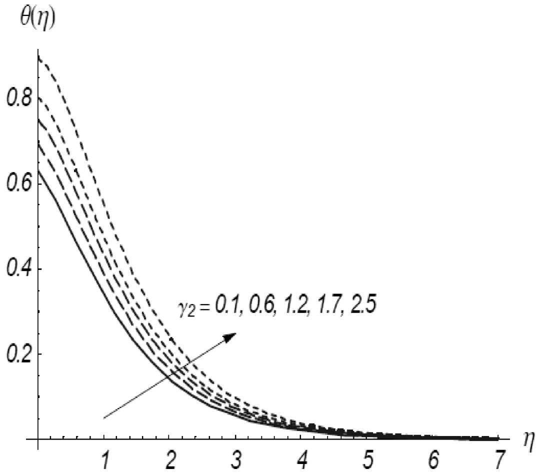

Fig. 7. Variation in temperature $\theta(\eta)$ vs η for different values of γ_2 when $M = 0.7$, $\Pr = 0.9$, $Le = 3.0$, $\gamma_1 = 0.5$, $Nt = Nb = 0.5$ and $Ec = 0.8$

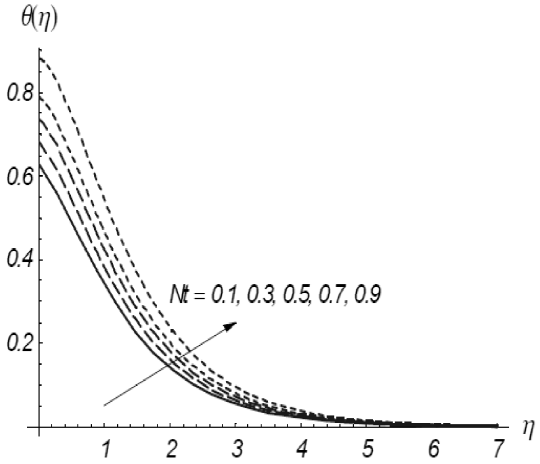

Fig. 8. Variation in temperature $\theta(\eta)$ vs η for different values of Nt when $M = 0.7$, $\Pr = 0.9$, $Le = 3.0$, $\gamma_1 = \gamma_2 = 0.5$, $Nb = 0.5$ and $Ec = 0.8$

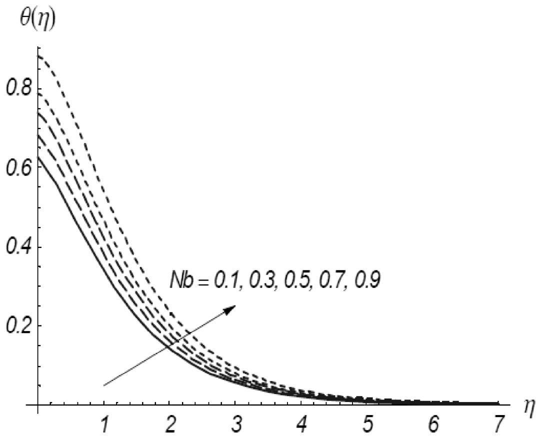

Fig. 9. Variation in temperature $\theta(\eta)$ vs η for different values of Nb when $M = 0.7$, $\Pr = 0.9$, $Le = 3.0$, $\gamma_1 = \gamma_2 = 0.5$, $Nt = 0.5$ and $Ec = 0.8$

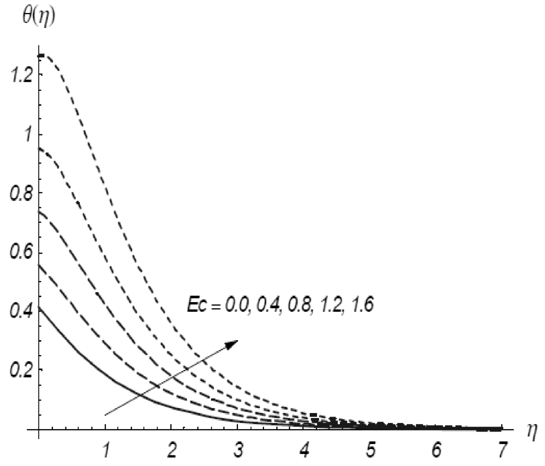

Fig. 10. Variation in temperature $\theta(\eta)$ vs η for different values of Ec when $M = 0.7$, $\Pr = 0.9$, $Le = 3.0$, $\gamma_1 = \gamma_2 = 0.5$ and $Nt = Nb = 0.5$

Figures 11–17 present the influences of M, Pr, Le, γ_1, γ_2, Nt and Nb on the dimensionless concentration $\phi(\eta)$. The higher values of magnetic parameter M leads to an increase in the concentration profile and its related layer thickness. The effects of magnetic parameter on the dimensionless temperature and concentration are similar (see Figs. 4 and 11). It is examined from Fig. 12 that concentration boundary layer thickness is thinner for the higher values of Prandtl number Pr. Comparison of Figs. 6 and 12 demonstrates that both temperature and concentration decrease through an increase in Prandtl number but the decrease in concentration is seen more dominant as observed for the temperature. The concentration distribution for different values of Lewis number Le is examined in Fig. 13. Here we have seen that an increase in Lewis number shows a rapid decrease in the concentration. Figures 14 and 15 elucidate that concentration is increasing when the values of Biot numbers γ_1 and γ_2 are increased. It is also seen from Fig. 14 that the concentration at the wall is lower corresponding to the $\gamma_2 = 0.1$ when $\gamma_1 = 0.1$. Figure 16 shows that the variation in concentration profile for various values of thermophoresis parameter Nt are similar to that analyzed in Fig. 8 but here the increase in concentration is more rapid. Figure 17 illustrates that the concentration profile is reduced when there is an increase in Brownian motion parameter Nb. Here we analyzed that the variation in concentration at $Nb = 0.1$, 0.3 is higher in comparison to the values of $Nb = 0.5$, 0.7 and 0.9.

Table 1 is computed for the numerical values of $-f''(0)$, $-\theta'(0)$ and $-\phi'(0)$ when $\hbar_f = \hbar_\theta = \hbar_\phi = -1.0$, $M = 0.4$, $\Pr = 0.9$, $Le = 2.0$, $Nt = Nb = 0.4$, $\gamma_1 = \gamma_2 = 1.0$ and $Ec = 0.8$ at different order of HAM approximations. One can see that the values of $-f''(0)$ repeated from 10th-order of HAM approximations while the values $-\theta'(0)$ and $-\phi'(0)$ converge from 31th-order of deformations. It is also examined from this Table that 31th-order of HAM approximations are required for a convergent series solutions of temperature and concentration. Table 2 provides the numerical values of skin-friction coefficient $-f''(0)$ for different values of magnetic

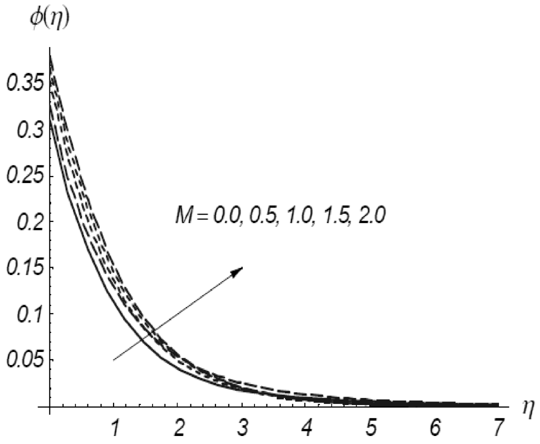

Fig. 11. Variation in concentration $\phi(\eta)$ vs η for different values of M when $\Pr = 0.9$, $Le = 3.0$, $\gamma_1 = \gamma_2 = 0.5$, $Nt = Nb = 0.5$ and $Ec = 0.8$

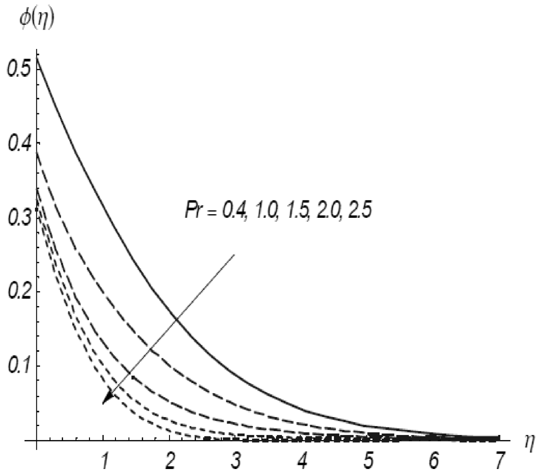

Fig. 12. Variation in concentration $\phi(\eta)$ vs η for different values of Pr when $M = 0.4$, $Le = 3.0$, $\gamma_1 = \gamma_2 = 0.5$, $Nt = Nb = 0.5$ and $Ec = 0.8$

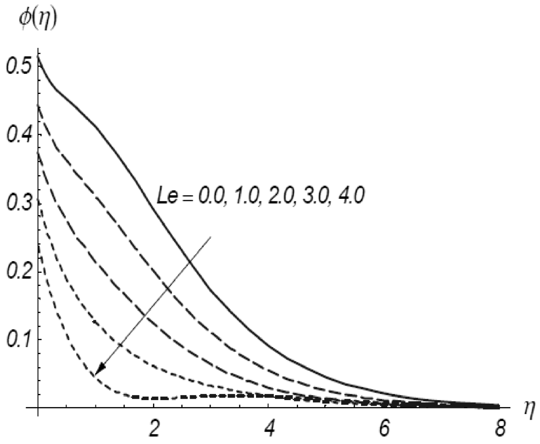

Fig. 13. Variation in concentration $\phi(\eta)$ vs η for different values of Le when $M = 0.7$, $\Pr = 0.9$, $\gamma_1 = \gamma_2 = 0.5$, $Nt = Nb = 0.5$ and $Ec = 0.8$

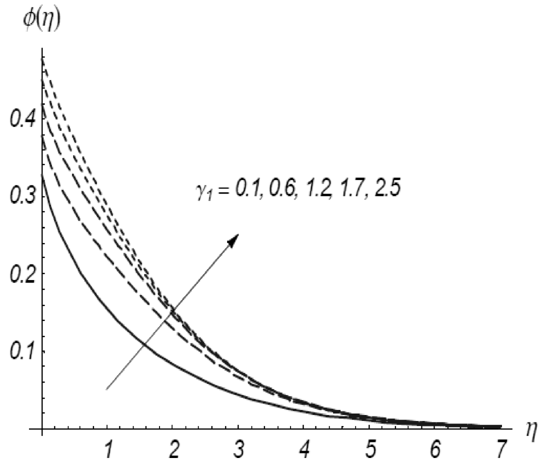

Fig. 14. Variation in concentration $\phi(\eta)$ vs η for different values of γ_1 when $M = 0.7$, $\Pr = 0.9$, $Le = 3.$, $\gamma_2 = 0.5$, $Nt = Nb = 0.5$ and $Ec = 0.8$

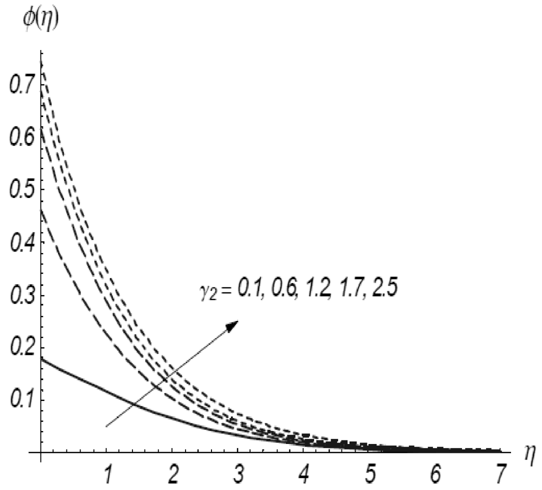

Fig. 15. Variation in concentration $\phi(\eta)$ vs η for different values of γ_2 when $M = 0.7$, $\Pr = 0.9$, $Le = 3.0$, $\gamma_1 = 0.5$, $Nt = Nb = 0.5$ and $Ec = 0.8$

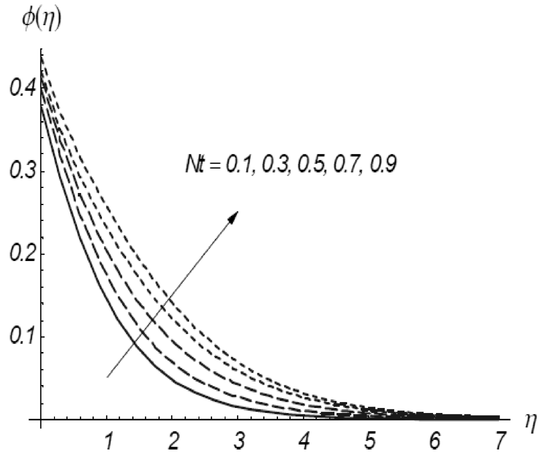

Fig. 16. Variation in concentration $\phi(\eta)$ vs η for different values of Nt when $M = 0.7$, $\Pr = 0.9$, $Le = 3.0$, $\gamma_1 = \gamma_2 = 0.5$, $Nb = 0.5$ and $Ec = 0.8$

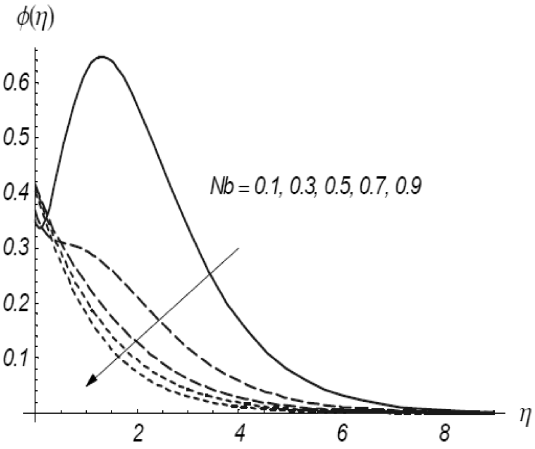

Fig. 17. Variation in concentration $\phi(\eta)$ vs η for different values of Nb when $M = 0.7$, $\Pr = 0.9$, $Le = 3.0$, $\gamma_1 = \gamma_2 = 0.5$, $Nt = 0.5$ and $Ec = 0.8$

Table 2
Numerical values of skin friction coefficient $-f''(0)$ for different values of M

M	$\hbar$	$-f''(0)$
0.0	−1.0	1.00000
0.2	−1.0	1.01980
0.5	−1.0	1.11803
0.8	−1.0	1.28063
1.0	−0.6	1.41421
1.2	−0.6	1.56205
1.5	−0.6	1.80303

Table 3
Numerical values of Nusselt number $-\theta'(0)$ for different values of M, Le, Nt, Nb, γ_1 and γ_2 when $\Pr = 1.2$ and $Ec = 0.5$

M	Le	Nt	Nb	γ_1	γ_2	$\hbar$	$-\theta'(0)$
0.0	1.5	0.2	0.2	0.3	0.3	−1.0	0.12060
0.5							0.08421
0.7							0.05163
0.3	1.0	0.2	0.2	0.3	0.3	-1.0	0.10714
	1.5						0.10714
	2.0						0.10714
0.3	1.5	0.1	0.2	0.3	0.3	-1.0	0.10994
		0.3					0.10427
		0.5					0.09835
0.3	1.5	0.2	0.1	0.3	0.3	-1.0	0.10905
			0.3				0.10521
			0.5				0.10132
0.3	1.5	0.2	0.2	0.1	0.3	-1.0	0.04647
				0.4			0.12787
				1.0			0.19541
0.3	1.5	0.2	0.2	0.3	0.1	-1.0	0.10943
					0.4		0.10626
					1.0		0.10294

parameter M. The values of skin-friction coefficient are smaller for the lower values of M. For $M = 0.0$, there is no magnetohydrodynamic flow. The numerical values of local Nusselt and Sherwood numbers $-\theta'(0)$ and $-\phi'(0)$ for different values of M, Le, Nt, Nb, γ_1 and γ_2 are computed in the Tables 3 and 4. The values of $-\theta'(0)$ and $-\phi'(0)$ are quite opposite for increasing values of M and Le. We have seen that the decrease in $-\theta'(0)$ corresponding to the higher values of Le are very small. The values of local Nusselt number are decreased with an increase in Nt and Nb. The values of local Sherwood number are increased by increasing Nb. To validate our solutions, we computed the values in Table 5. This Table guarantees that our solutions are correct because an excellent agreement is noted with the previous results in the limiting cases.

Table 4
Numerical values of Sherwood number $-\phi'(0)$ for different values of M, Le, Nt, Nb, γ_1 and γ_2 when $\Pr = 1.2$ and $Ec = 0.5$

M	Le	Nt	Nb	γ_1	γ_2	$\hbar$	$-\phi'(0)$
0.0	1.5	0.2	0.2	0.3	0.3	-1.0	0.22066
0.5							0.22953
0.7							0.23742
0.3	1.0	0.2	0.2	0.3	0.3	-1.0	0.20284
	1.5						0.22396
	2.0						0.23791
0.3	1.5	0.1	0.2	0.3	0.3	-1.0	0.22230
		0.3					0.22628
		0.5					0.23319
0.3	1.5	0.2	0.1	0.3	0.3	-1.0	0.22547
			0.3				0.22347
			0.5				0.22308
0.3	1.5	0.2	0.2	0.1	0.3	-1.0	0.23318
				0.4			0.22082
				1.0			0.21066
0.3	1.5	0.2	0.2	0.3	0.1	-1.0	0.09019
					0.4		0.27494
					1.0		0.46576

Table 5
Comparison of values of $-\theta'(0)$ for different values of Pr with the previous existing results when $Nt = Nb = 0.0$ and $\gamma_1 = 1000$

Pr	$-\theta'(0)$		
	Present results	[5]	[6]
0.07	0.06637	0.0663	0.0663
0.20	0.61913	0.1691	0.1691
0.70	0.45395	0.4539	0.4539
2.00	0.91132	0.9113	0.9113

5. Concluding remarks

Effects of convective heat and mass conditions in the MHD boundary layer flow of nanofluid over a stretching surface with viscous dissipations and Joule heating are studied. The main observations of the presented analysis are listed below.

1. Higher values of magnetic parameter M enhance the temperature and concentration profiles.
2. A decrease in concentration distribution is more pronounced in comparison with temperature for the increasing values of Prandtl number Pr.

3. Temperature and thermal boundary layer thickness are increasing functions of Eckert number Ec.
4. Both temperature and concentration fields are increased by increasing the values of Biot numbers γ_1 and γ_2.
5. An increase in temperature is more dominant by increasing the values of a thermophoresis parameter in comparison with the Brownian motion parameter.
6. Concentration boundary layer thickness is thinner for higher values of Lewis number Le.
7. Increasing values of magnetic parameter M leads to an increase in the skin-friction coefficient.

REFERENCES

[1] A. Sharma, V.V. Tyagi, C.R. Chen, and D. Buddhi, "Review on thermal energy storage with phase change materials and applications", *Renew. Sustain. Energy Rev.* 13, 318–345 (2009).

[2] S. Kakac and A. Pramuanjaroenky, "Review of convective heat transfer enhancement with nanofluids", *Int. J. Heat Mass Transfer* 52, 3187–3196 (2009).

[3] S.U.S. Choi, "Enhancing thermal conductivity of fluids with nanoparticles, in *Proc. 1995 ASME Int. Mechanical Engineering Congress and Exposition* ASME, FED 231/ MD 66, 99–105 (1995).

[4] S.U.S. Choi, Z.G. Zhang, W. Yu, F.E. Lockwood, and E.A. Grulke, "Anomalously thermal conductivity enhancement in nanotube suspensions", *Appl. Phys. Lett.* 79, 2252-2254 (2001).

[5] O.D. Makinde and A. Aziz, "Boundary layer flow of nanofluid past a stretching sheet with a convective boundary condition", *Int. J. Therm. Sci.* 50, 1326-1332 (2011).

[6] A. Alsaedi, M. Awais, and T. Hayat, "Effects of heat generation/absorption on stagnation point flow of nanofluid over a surface with convective boundary conditions", *Commun. Nonlinear Sci. Numer. Simulat.* 17, 4210–4223 (2012).

[7] M.M. Rashidi, S. Abelman, and N. F. Mehr, "Entropy generation in steady MHD flow due to a rotating porous disk in a nanofluid", *Int. J. Heat Mass Transfer* 62, 515–525 (2013).

[8] M. Turkyilmazoglu, "Exact analytical solutions for heat and mass transfer of MHD slip flow in nanofluids", *Chem. Engin. Sci.* 84, 182–187 (2012).

[9] S. Nadeem and C. Lee, "Boundary layer flow of nanofluid over an exponentially stretching surface", *Nanoscale Research Lett.* 7, 94 (2012).

[10] O.D. Makinde, W.A. Khan, and Z.H. Khan, "Buoyancy effects on MHD stagnation point flow and heat transfer of a nanofluid past a convectively heated stretching/shrinking sheet", *Int. J. Heat Mass Transfer,* 62, 526–533 (2013).

[11] M. Mustafa, M.A. Farooq, T. Hayat, and A. Alsaedi, "Numerical and series solutions for stagnation-point flow of nanofluid over an exponentially stretching sheet", *Plos One* 8, e61859 (2013).

[12] W.N. Mutuku-Njane and O.D. Makinde, "Combined effect of buoyancy force and Navier slip on MHD flow of nanofluid over a convectively heated vertical porous plate", *Scientific Worrld J.* 2013, 725643 (2013).

[13] O.D. Makinde, "Effects of viscous dissipation and Newtonian heating on boundary layer flow of nanofluids over a flat plate", *Int. J. Numer. Methods Heat Fluid Flow* 23, 1291–1303 (2013).

[14] O.D. Makinde, "Computational modelling of nanofluids flow over a convectively heated unsteady stretching sheet", *Current Nanoscience* 9, 673–678 (2013).

[15] A.V. Kuznetson and D.A. Nield, "The Cheng-Minkowycz problem for natural convective boundary layer flow in a porous medium saturated by a nanofluid", *Int. J. Heat Mass Transfer* 65, 682–685 (2013).

[16] W.N. Mutuku-Njane and O.D. Makinde, "MHD nanofluid flow over a permeable vertical plate with convective heating", *J. Comput. Theore. Nanoscience* 11, 667–675 (2014).

[17] G.C. Layek, S. Mukhopadhyay, and S.A. Samad, "Heat and mass transfer analysis for boundary layer stagnation-point flow towards a heated porous stretching sheet with heat absorption/generation and suction/blowing", *Int. Commun. Heat Mass Transfer* 34, 347–356 (2007).

[18] O.D. Makinde, "On MHD boundary-layer flow and mass transfer past a vertical plate in a porous medium with constant heat flux", *Int. J. Numer. Methods Heat Fluid Flow* 19, 546–554 (2009).

[19] S.S. Motsa, S. Shateyi, and Z. Makukula, "Homotopy analysis of free convection boundary layer flow with heat and mass transfer", *Chem. Eng. Commun.* 198, 783–795 (2011).

[20] K. Bhattacharyya, "Dual solutions in boundary layer stagnation-point flow and mass transfer with chemical reaction past a stretching/shrinking sheet", *Int. Commun. Heat Mass Transfer* 38, 917–922 (2011).

[21] M. Mahmood, S. Asghar, and M.A. Hossain, "Transient mixed convection flow arising due to thermal and mass diffusion over porous sensor surface inside squeezing horizontal channel", *Appl. Math. Mech.-Engl. Ed.* 34, 97–112 (2013).

[22] M. Turkyilmazoglu, "Heat and mass transfer of MHD second order slip flow", *Comput. Fluids* 71, 426–434 (2013).

[23] S.A. Shehzad, F.E. Alsaadi, S.J. Monaquel, and T. Hayat, "Soret and Dufour effects on the stagnation point flow of Jeffery fluid with convective boundary condition", *Eur. Phys. J. Plus* 128, 56 (2013).

[24] M. Turkyilmazoglu and I. Pop, "Soret and heat source effects on the unsteady radiative MHD free convection flow from an impulsively started infinite vertical plate", *Int. J. Heat Mass Transfer* 55, 7635–7644 (2012).

[25] M.M. Rashidi, M. Ali, N. Freidoonimehr, and F. Nazari, "Parametric analysis and optimization of entropy generation in unsteady MHD flow over a stretching rotating disk using artificial neural network and particle swarm optimization algorithm", *Energy* 55, 497–510 (2013).

[26] L. Rundora and O.D. Makinde, "Effects of suction/injection on unsteady reactive variable viscosity non-Newtonian fluid flow in a channel filled with porous medium and convective boundary conditions", *J. Petroleum Sci. Eng.* 108, 328–335 (2013).

[27] S.A. Shehzad, A. Alsaedi, and T. Hayat, "Hydromagnetic steady flow of Maxwell fluid over a bidirectional stretching surface with prescribed surface temperature and prescribed surface heat flux", *Plos One* 8, e68139 (2013).

[28] S.J. Liao, *Homotopy Analysis Method in Nonlinear Differential Equations*, Springer & Higher Education Press, Heidelberg, 2012.

[29] M. Turkyilmazoglu, "Solution of the Thomas-Fermi equation with a convergent approach", *Commun. Nonlinear Sci. Numer. Simulat.* 17, 4097–4103 (2012).

[30] W. Zhang, Y.H. Qian, and S.K. Lai, "Extended homotopy analysis method for multi-degree-of-freedom non-autonomous nonlinear dynamical systems and its application", *Acta Mech.* 223, 2537–2548 (2012).

[31] M.M. Rashidi, M. Keimanesh, and S.C. Rajvanshi, "Study of pulsatile flow in a porous annulus with the homotopy analysis

method", *Int. J. Numer. Methods Heat Fluid Flow* 22, 971–989 (2012).

[32] S. Abbasbandy, M.S. Hashemi, and I. Hashim, "On convergence of homotopy analysis method and its application to fractional integro-differential equations", *Quaestiones Mathematicae* 36, 93–105 (2013).

[33] T. Hayat, M. Waqas, S.A. Shehzad, and A. Alsaedi, "Mixed convection radiative flow of Maxwell fluid near a stagnation point with convective condition", *J. Mech.* 29, 403-409 (2013).

[34] M. Ramzan, M. Farooq, A. Alsaedi, and T. Hayat, "MHD three-dimensional flow of couple stress fluid with Newtonian heating", *Eur. Phys. J. Plus* 128, 49 (2013).

[35] S.A. Shehzad, M. Qasim, T. Hayat, M. Sajid, and S. Obaidat, "Boundary layer flow of Maxwell fluid with power law heat flux and heat source", *Int. J. Numer. Methods Heat Fluid Flow* 23, 1225–1241 (2013).

[36] H.N. Hassan and M.M. Rashidi, "An analytic solution of micro polar flow in a porous channel with mass injection using homotopy analysis method", *Int. J. Numer. Methods Heat Fluid Flow* 24, 419–437 (2014).

[37] T. Hayat, S.A. Shehzad, S. Al-Mezel, and A. Alsaedi, "Three-dimensional flow of an Oldroyd-B fluid over a bidirectional stretching surface with prescribed surface temperature and prescribed surface heat flux", *J. Hydrol. Hydromech.* 62, 117–125 (2014).

[38] T. Hayat, S. Asad, and A. Alsaedi, "Flow of variable thermal conductivity fluid due to inclined stretching cylinder with viscous dissipation and thermal radiation", *Appl. Math. Mech.* 35, 717–728 (2014).

[39] H. Schlichting, *Boundary Layer Theory*, McGraw-Hill, New York, 1964.